

C.Sefa Dikmen¹, M.Nur Yüksel¹, M.Yumuşak¹

¹Roketsan Inc., Kemalpasa Mh.,Şehit Yüzbaşı Adem Kutlu Sk., No:21, Ankara, Elmadağ, Türkiye

Abstract

The aerothermodynamic effects of high-enthalpy hypersonic flows are considered as vital for hypersonic flow studies. The change between perfect gas flow and chemically reacting flow at hypersonic Mach numbers may be detrimental; therefore, analysts and designers should carefully investigate these changes starting from the basic test geometries. A series of CFD runs are executed using a cylindrical geometry and a double-cone geometry. The results do not only demonstrate the effect of thermochemical changes on the flow field but also how two commercial flow solvers such as ANSYS Fluent and METACOMP CFD++ perform under similar numerical conditions. It is clear that ignoring mentioned effects at critical locations may not be acceptable and flow properties just around the surface of the object and surface loadings may be missed.

Keywords: Hypersonic, Fluent, CFD++, aerothermodynamic, nonequilibrium

1. Introduction

Although its first research efforts go to 20th century, hypersonic flow and hypersonic vehicles take attention of many researchers and defense industries of many countries in the last years. Due to its challenging working environment, the term of hypersonic brings many scientific disciplines together such as aerodynamics, thermal and chemical. CFD modelling is one of the most critical parts of hypersonic research because testing everything is not possible and feasible for such a flow regime. For this reason, CFD modelling should be sufficiently accurate to model shock patterns, shock-boundary-layer-interactions (SBLI) and separation regions.

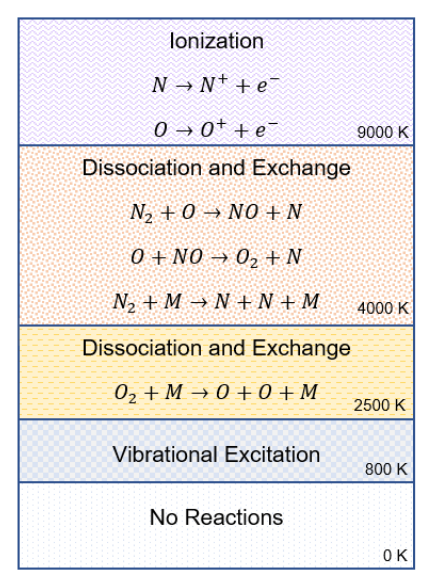


Figure 1- Chemical Change of Flow Composition under Different Thermal Conditions: Adapted From [1]

Before conducting any design and analysis study, the CFD methodology should be decided and validated. Two simple experimental geometry, which are HEG cylinder and CUBRC double cone can be counted as suitable for this purpose with their open-source literature data. A typical cylinder geometry is required to see bow-shocks and stagnation region heating, a double cone geometry is required to see shocks, interactions and separations around ramp corners.

These two geometries have surface pressure and heat flux measurements available to compare with CFD results. Since CFD modelling can start with simple models and go towards more complicated models including multiple species and chemical reaction effects, present study will handle them one by one to show differences. Figure 1 explains how the composition of the air changes if the temperature increases. The change of the gas composition changes the gas properties and there occurs chemical reactions among the new composition. All of these changes require different approaches in CFD compared with a standard fluid problem. Two simple test geometry can be seen at Figure 2 and Figure 3.



Figure 2- HEG Cylinder Test Geometry [2]

Figure 3- CUBRC Double Cone Geometry [3]

2. Methodology

2.1 Freestream Conditions

Freestream conditions used in CFD are obtained from experimental references. Although there exist many experimental test conditions, relatively challenging test conditions are selected to force CFD solvers for observations. Test conditions for both geometries can be seen at Table 1 and Table 2.

Table 1- HEG Cylinder Test Conditions [2]

Static Pressure (Pa)	Static Temperature (K)	Mach	Density(kg/m³)	Enthalpy (MJ/kg)
476	901	8.98	1.547E-3	22.4
Y[N2]	Y[O2]	Y[NO]	Y[N]	Y[O]
0.7543	0.00713	0.01026	6.5E-7	0.2283

Table 2- CUBRC Double Cone Test Conditions [4]

Static Pressure (Pa)	Static Temperature (K)	Mach	Density(kg/m³)	Enthalpy (MJ/kg)
77	521	13.23	0.511	18.7
Y[N2]	Y[O2]	Y[NO]	Y[N]	Y[O]
0.765	0.235	0	0	0

2.2 Computational Domain

Computational domain of both geometries is prepared by structured meshing. First layer thickness is decided by y+<1 criterion, and it is 4E-6m. HEG cylinder geometry is composed of 56000 cells while double cone geometry is composed of 176000 cells. Since the grid is intense near the surface, the visibility of the whole domain is hard, so figures are not added.

2.3 Boundary Conditions

Boundary conditions are defined based on Table 1 and Table 2. Far-field boundary of the domain is defined using static temperature, pressure and Mach number. The wall is taken as the isothermal wall, which is 300K and wall temperature is equal to vibrational temperature for the use of two temperature model.

2.4 Governing Equations of the Flow

The generalized 3D system of viscous Navier-Stokes equations in thermochemical non-equilibrium can be written as follows. It should be noted that the third dimension is not valid in the present paper due to 2D computations.

$$\frac{\partial \alpha}{\partial t} + \frac{\partial \beta}{\partial x} + \frac{\partial \theta}{\partial y} + \frac{\partial \varphi}{\partial z} - \left(\frac{\partial \beta_{visc}}{\partial x} + \frac{\partial \theta_{visc}}{\partial y} + \frac{\partial \varphi_{visc}}{\partial z}\right) = S$$

$$\alpha = \begin{bmatrix} \rho_{i} \\ \vdots \\ \rho_{tns} \\ \rho_{u} \\ \rho_{v} \\ \rho_{w} \\ \rho_{E} \\ \rho e_{ve} \end{bmatrix}, \beta = \begin{bmatrix} u\rho_{i} \\ \vdots \\ u\rho_{tns} \\ \rho + \rho u^{2} \\ \rho uv \\ \rho uw \\ \rho uH \\ u\rho e_{ve} \end{bmatrix} \theta = \begin{bmatrix} v\rho_{i} \\ \vdots \\ v\rho_{tns} \\ \rho uv \\ p + \rho v^{2} \\ \rho vw \\ \rho vH \\ v\rho e_{ve} \end{bmatrix} \varphi = \begin{bmatrix} w\rho_{i} \\ \vdots \\ w\rho_{tns} \\ \rho uw \\ \rho vw \\ \rho vw \\ p + \rho w^{2} \\ \rho wH \\ w\rho e_{ve} \end{bmatrix} S = \begin{bmatrix} \dot{\omega}_{i} \\ \vdots \\ \dot{\omega}_{tns} \\ 0 \\ 0 \\ 0 \\ \dot{\omega}_{ve} \end{bmatrix}$$

Above, α demonstrates the conservative variables and β , θ and φ are inviscid flux vectors. Terms with the subscript of "visc" are viscous flux vectors. "S" demonstrates source terms such as body forces and energy sources. The subscript of "tns" means the total number of species, "ve" means vibrational-electronic and "tr" means translational-rotational.

The general set of equation includes terms which indicate the internal energy storage of the species. "e" term means internal energy and " h_0 " term means species heat of formation.

$$e_{int} = e_{tr}T_{tr} + e_{rot}T_{tr} + e_{vih}T_{ve} + e_{elec}T_{ve} + h_0$$

For the species transport physics, only volumetric reactions are used. Chemical reactions consider the five-species air model of Park. [5] There is no wall-surface or particle-surface reactions included. It is mentioned that turbulence model of the flow is chosen as Spalart-Allmaras. There is no chemistry-turbulence interaction in the setup, and the solver computes only the Arrhenius rate and finite rate kinetics are directly used. Following equation indicates the reaction where " $v_{i,r}$ " is stoichiometric coefficient for product i, " k_{fr} and k_{br} " are forward and backward rate constants in the reaction "r". " M_i " demonstrates species in the reaction.

$$\sum_{i=1}^{tns} v_{i,r} M_i \underset{k_{br}}{\overset{k_{fr}}{\longleftrightarrow}} \sum_{i=1}^{tns} v_{i,p} M_i$$

Considering the complexity of chemistry and hypersonic flow, it is a suitable choice to get rid of computationally expensive runs for the scape of present study. If the flow problem was radically different such as partially stirred reactor or scramjet combustor flames, it would be wiser to include the model of eddy-dissipation concepts and to model turbulence-chemistry interaction.

2.5 Thermochemistry Model

Thermochemistry model can be seen in Table 3. It is adopted up to the solver's requirements.

Ċ ϵ/k β A_5 Reaction A_1 A_2 A_3 A_4 η (m3/kg·mole·s) (K) 3.70×10^{18} $N_2 + N_2 \rightarrow N + N + N_2$ -1.6113,200 0.5 0.5 10.81 -12.610.683 -0.1180.006 $N_2 + N \rightarrow N + N + N$ 1.11×10^{19} 113,200 -1.60.5 0.5 10.81 -12.610.683 -0.1180.006 3.70×10^{18} $N_2 + NO \rightarrow N + N + NO$ -1.6113,200 0.5 0.5 10.81 -12.610.683-0.1180.006 3.70×10^{18} $N_2 + O_2 \rightarrow N + N + O_2$ -12.61-1.6113,200 0.5 0.5 10.81 0.683 -0.1180.006 1.11×10^{19} $N_2 + O \rightarrow N + N + O$ 113,200 0.5 0.5 -12.61-0.118-1.610.81 0.6830.006 3.18×10^{10} $N_2 + O \rightarrow NO + N$ 0.1 -4.82837,700 1.0 0.02.349 0.455-0.0750.004 2.75×10^{16} $O_2 + N_2 \rightarrow O + O + N_2$ -1.059,500 0.5 0.5 8.243 -4.127-0.6160.093 -0.005 8.25×10^{16} $O_2 + N \rightarrow O + O + N$ 59,500 -0.005-1.00.5 0.5 8.243 -4.127-0.6160.093 2.75×10^{16} $O_2 + NO \rightarrow O + O + NO$ -1.059,500 0.5 0.5 8.243 -4.127-0.6160.093-0.005 $O_2 + O_2 \rightarrow O + O + O_2$ 2.75×10^{16} -1.059,500 0.5 0.5 8.243 -4.127-0.6160.093 -0.005 8.25×10^{16} $O_2 + O \rightarrow O + O + O$ -1.059,500 0.5 0.5 8.243 -4.127-0.6160.093 -0.005 2.16×10^{5} $NO + O \rightarrow N + O_2$ 19,220 0.843 0.007 1.29 1.0 0.0 0.215 -3.657-0.136 2.30×10^{14} $NO + N_2 \rightarrow N + O + N_2$ -0.575,500 0.5 0.5 8.457 -7.7840.228 -0.0430.002 2.30×10^{14} $NO + NO \rightarrow N + O + NO$ -0.575,500 0.5 0.5 8.457 -7.7840.228-0.0430.002 2.30×10^{14} 8.457 $NO + O_2 \rightarrow N + O + O_2$ -0.575,500 0.5 0.5 -7.7840.228-0.0430.002 4.60×10^{14} $NO + N \rightarrow N + O + N$ -0.575,500 0.5 0.5 8.457 -7.7840.228-0.0430.002 4.60×10^{14} $NO + O \rightarrow N + O + O$ -0.575,500 0.5 0.5 8.457 -7.7840.228-0.0430.002

Table 3- Thermochemistry Model [3]

Notes: $k_f = CT_a^{\eta} e^{-c/kT_a}$, $T_a = T^{\alpha} T_{\text{vib}}^{\beta}$, $k_e = \exp(A_1 + A_2 z + A_3 z^2 + A_4 z^3 + A_5 z^4)$ where $z = 10^4/T$.

For the density-based solver, two temperature model is used to simulate thermal non-equilibrium effects of the hypersonic flow. It is theoretically known that the flow field can be obtained better compared to one-temperature model because certain levels of temperature of the flow cause that species do not only have translational and rotational modes but also, they have vibrational and electronic modes.

The Blottner's curve fit is used for the calculation of viscosity, the Eucken's relation is used for the calculation of species' thermal conductivities and constant Lewis number is used for the modelling of diffusivity coefficient. In the case of very high flow speeds and ionization, Gupta's mixing law is appropriate.

2.6 Methodology Related to Solvers

In this study, two commercial solvers, which are ANSYS Fluent 2022R2 and Metacomp CFD++ 20.1 are used.

In ANSYS Fluent, ideal gas model, thermal non-equilibrium model and thermochemical non-equilibrium model are investigated. Park's 5-species-air model [5] is chosen for multi-species purposes. Density based solver, implicit formulation and AUSM flux-splitting are used. Turbulence model is one-equation Spalart-Allmaras model with viscous heating. The discretization is second order upwind without any first-order blending. CFL number is adaptively adjusted based on solution and residuals.

In Metacomp CFD++, the general methodology is similar to Fluent with slight differences. HLLC method is used compared to AUSM. Other user-selected options are kept similar between two solvers as possible.

It should be noted that AUSM+ formulation is known as a cure for problems related to carbuncle phenomenon. Since the geometry like HEG cylinder is prone to carbuncle, it is a suitable choice to use AUSM+.

3. Results

3.1 ANSYS Fluent Results

Results can be evaluated by using contours and plots. Flow field can be seen at contours. The bow shock in front of the surface and very high temperature levels are visible in Figure 4. Since two temperature model is activated, there exists a Vibrational-Electronic temperature flow field. The difference between Translational-Rotational temperature and Vibrational-Electronic temperature is compatible with the result given in literature. [6]

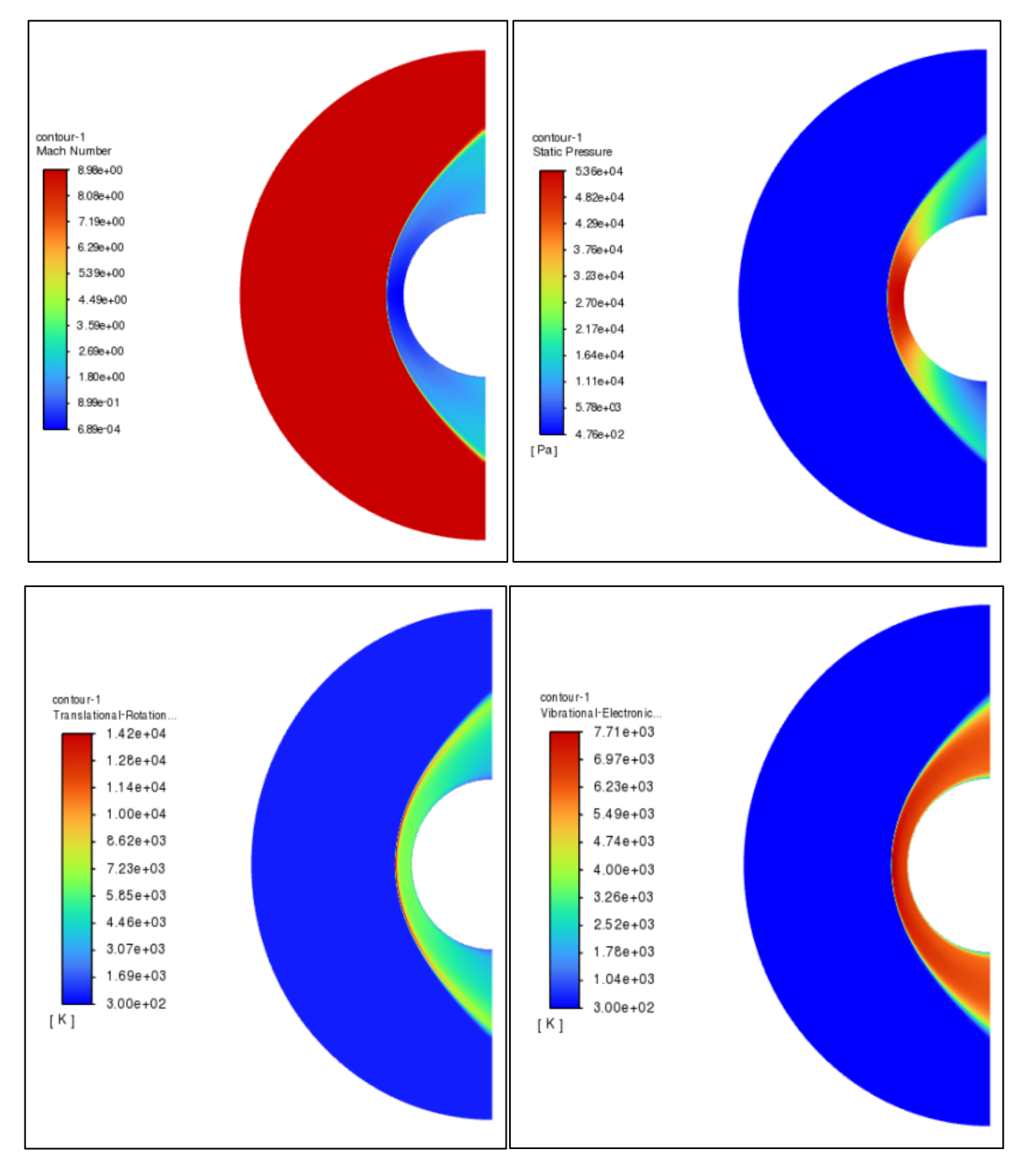


Figure 4- HEG Cylinder Aerothermal Flow Field-Fluent

Also, there is a very thin boundary layer on the cylinder surface, which can be seen from the Mach number contour. There is a strong Mach number change indicating the shock wave ahead of the cylinder. Translational-Rotational and Vibrational-Electronic temperatures are almost identical around stagnation region. This fact changes rapidly away from the stagnation region because of the expansion.

One of the main purposes of this study is about the investigation of thermochemical nonequilibrium effects of hypersonic flows and Figure 5 demonstrates how composition differs from the initial state

due to the high temperature around the surface. Around stagnation region, single atomic N appears while O_2 is completely consumed. These findings are suitable to what Figure 1 states theoretically.

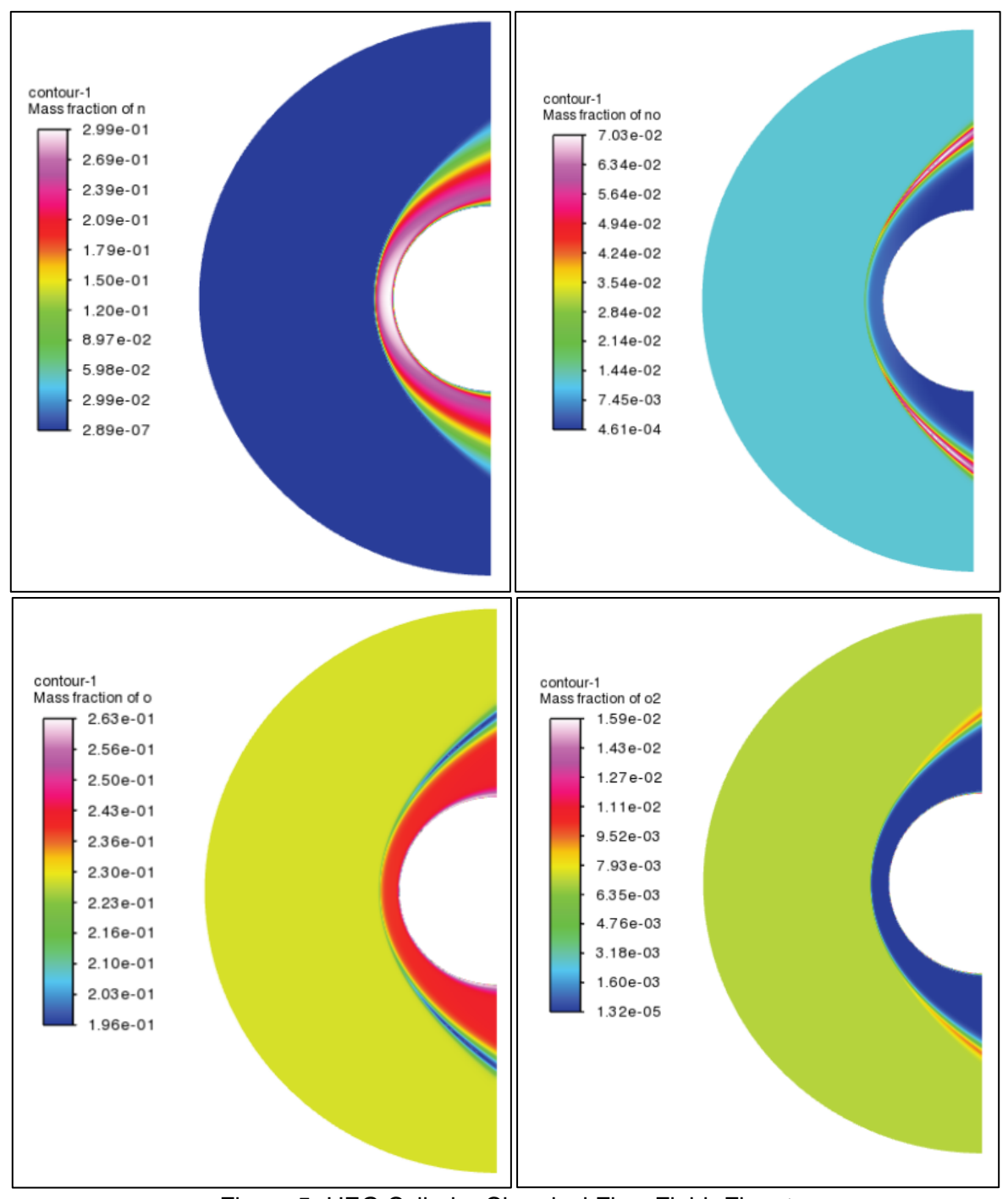


Figure 5- HEG Cylinder Chemical Flow Field- Fluent

Figure 6 indicates how different models perform around stagnation region of the cylinder for the surface pressure. Thermal and thermochemical nonequilibrium models predict better but all models display excellent agreement with the experimental data. It should be remembered that present conditions have very high enthalpy compared to other HEG experimental runs. However, the effect of different models is more visible for the heat flux case given in Figure 7. Thermochemical nonequilibrium model is the closest one to the experimental data while other models have remarkable deviations especially around stagnation region. Even thermochemical nonequilibrium model has some difference compared to experimental data but the amount of deviation seems in agreement with the literature results. When the literature is examined, only numerical setups with the fully catalytic for radicals. Consequently, present results are in agreement with the literature in case of non-catalytic setups while it is possible to approach towards experimental data for the stagnation heat flux if fully catalyticity is added.

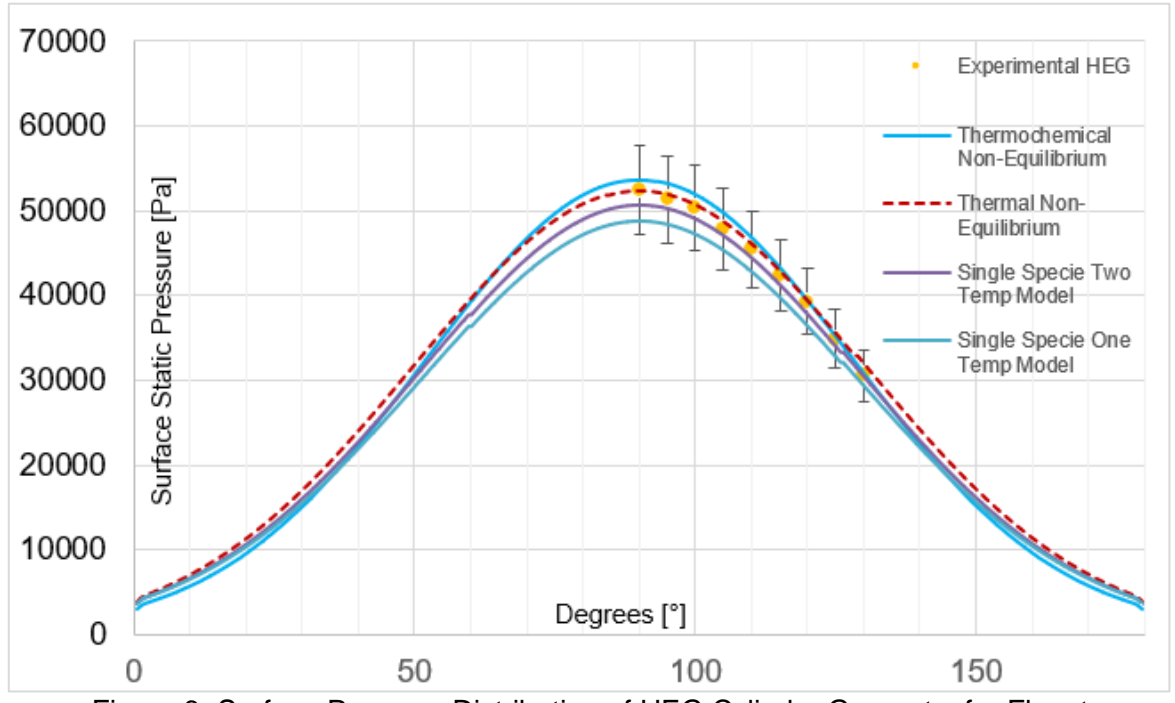


Figure 6- Surface Pressure Distribution of HEG Cylinder Geometry for Fluent

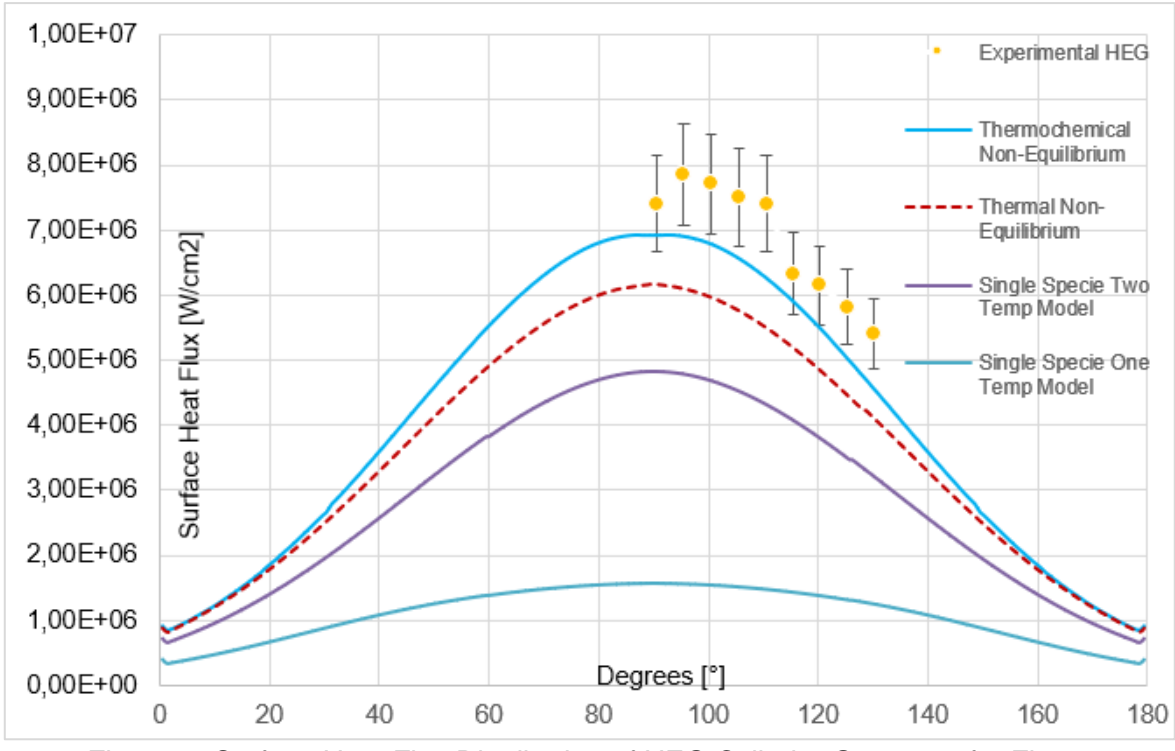


Figure 7- Surface Heat Flux Distribution of HEG Cylinder Geometry for Fluent

Another result which can be observed from Figure 6 and Figure 7 is the applicability of simpler models to more complex 3D real geometries. The biggest deviation between the thermochemical non-equilibirium model and other models occurs around the stagnation region for the heat flux, while results are almost identical for the static pressure. If a complex geometry is investigated aerodynamically, it may not be a "must" choice to model chemical effects to obtain aerodynamic flow field. If detailed surface heat transfer results are needed, this case is more efficient to model non-equilibrium effects.

More challenging results can be seen from Figure 8 and Figure 9 because double cone geometry causes significant physical phenomena around ramp intersections. Due to the triple point including SBLI, separation bubble and reattachment shock, strong flow gradients appear. As a result, pressure

and heat flux distribution demonstrate big spikes at results numerically.

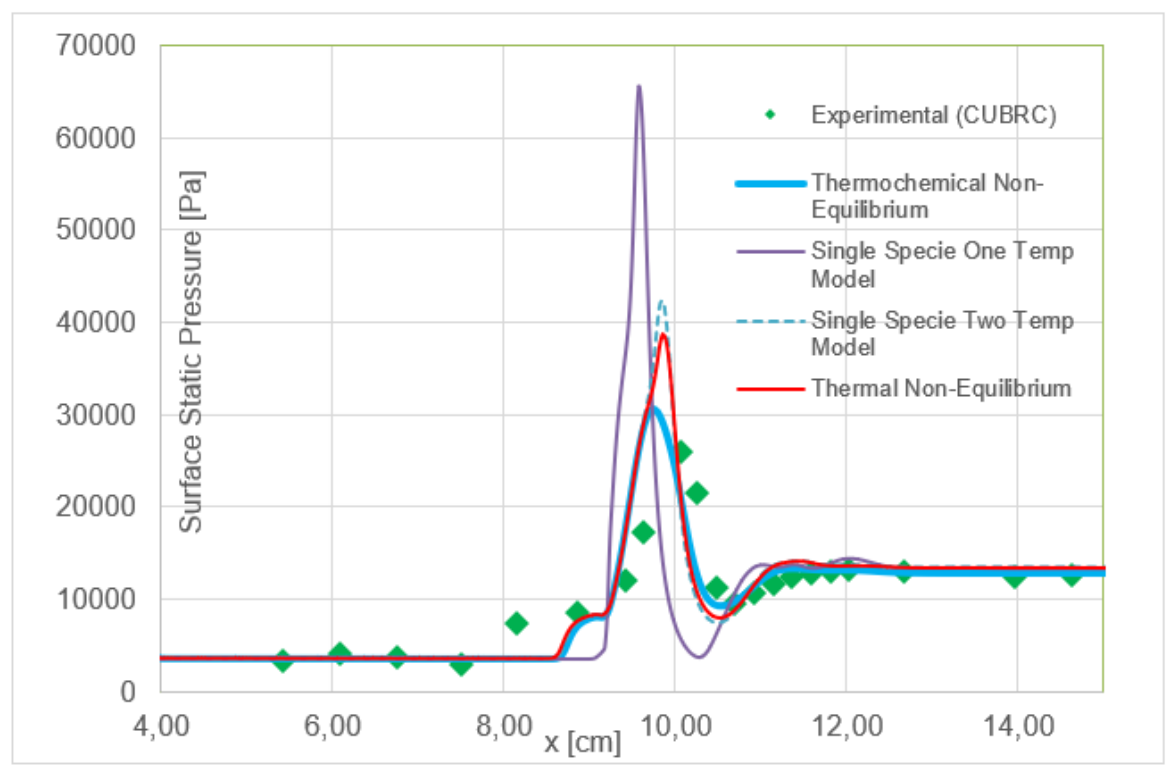


Figure 8- Surface Pressure Distribution of CUBRC Double Cone Geometry for Fluent

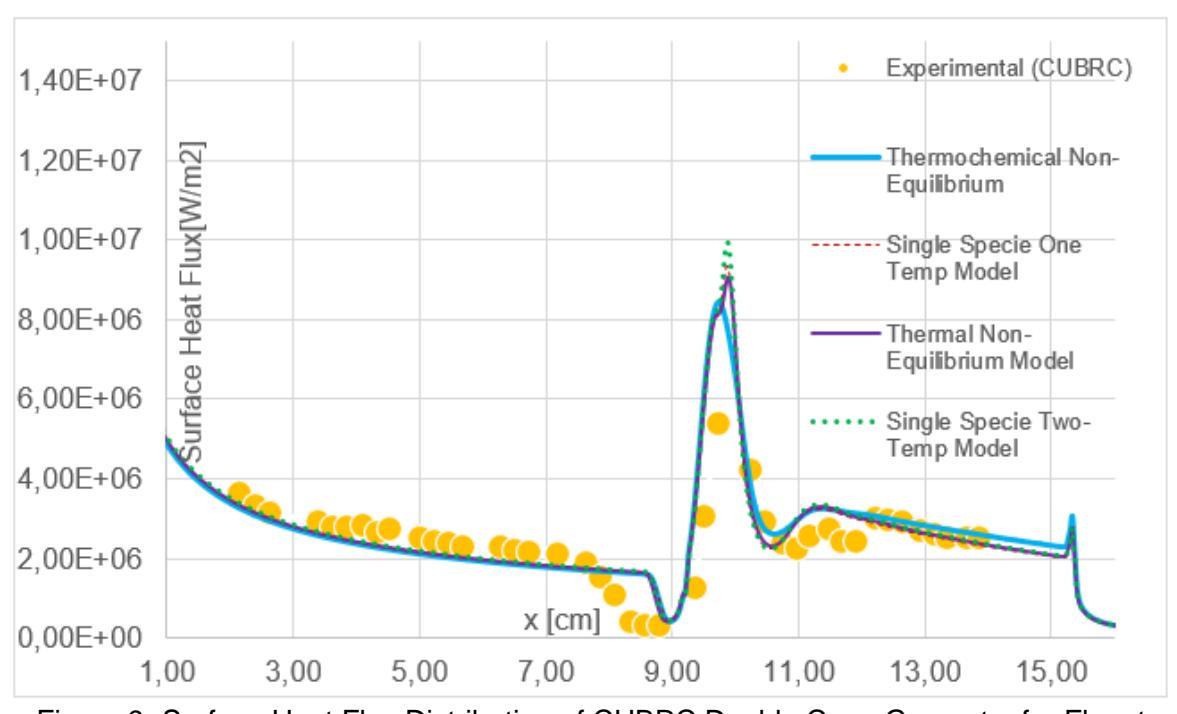


Figure 9- Surface Heat Flux Distribution of CUBRC Double Cone Geometry for Fluent

At this point, another observation should be mentioned. Experimental data is available at 9.6 cm and 10 cm for double cone geometry. When the maximum level of pressure and heat flux spikes are investigated, one of the possible reasons of the deviation may be the spacing of measurement devices. CFD calculations are made up to resolution of the solution grid, which has much more points compared to experiment. To be more precisely, there is no information about the point at 9.7 or 9.8 cm for the experimental data. The real trend may reach much higher levels. In general, CFD follows the experimental trend successfully, especially for the thermochemical nonequilibrium model.

3.2 METACOMP CFD++ Results

In this part, contours will not be demonstrated again because there is no visible difference between flow field of two solvers. Yet, differences can be seen at numerical surface pressure and heat flux plots so they will be demonstrated.

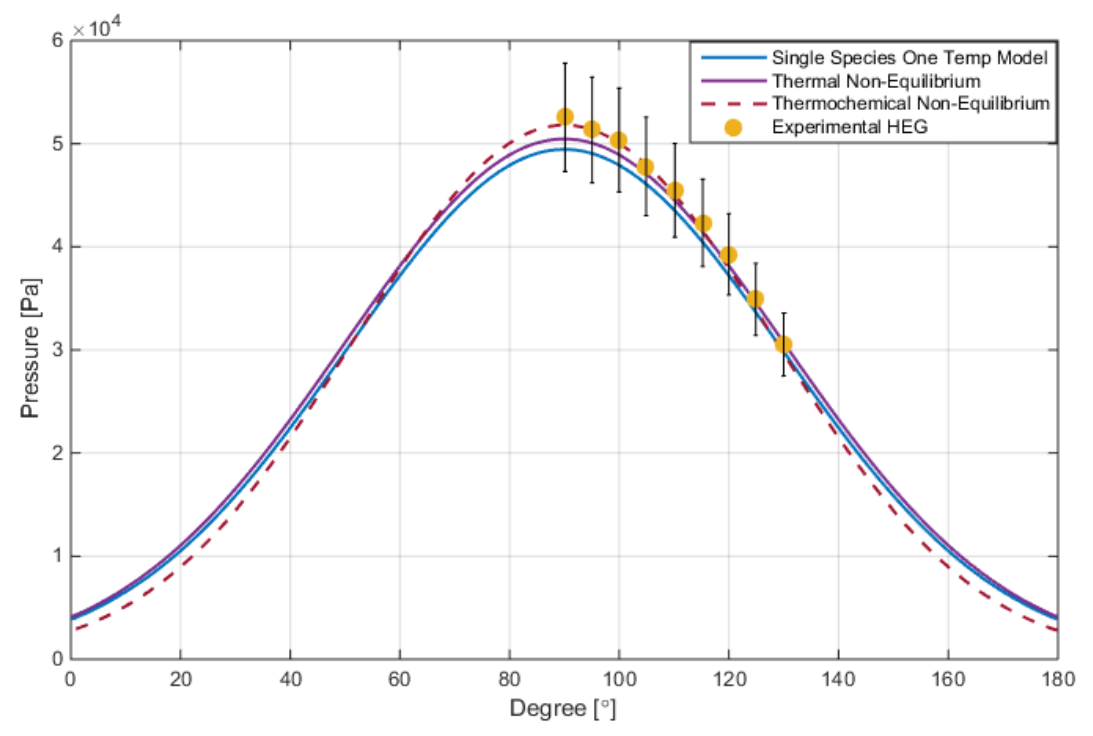


Figure 10- Surface Pressure Distribution of HEG Cylinder Geometry for CFD++

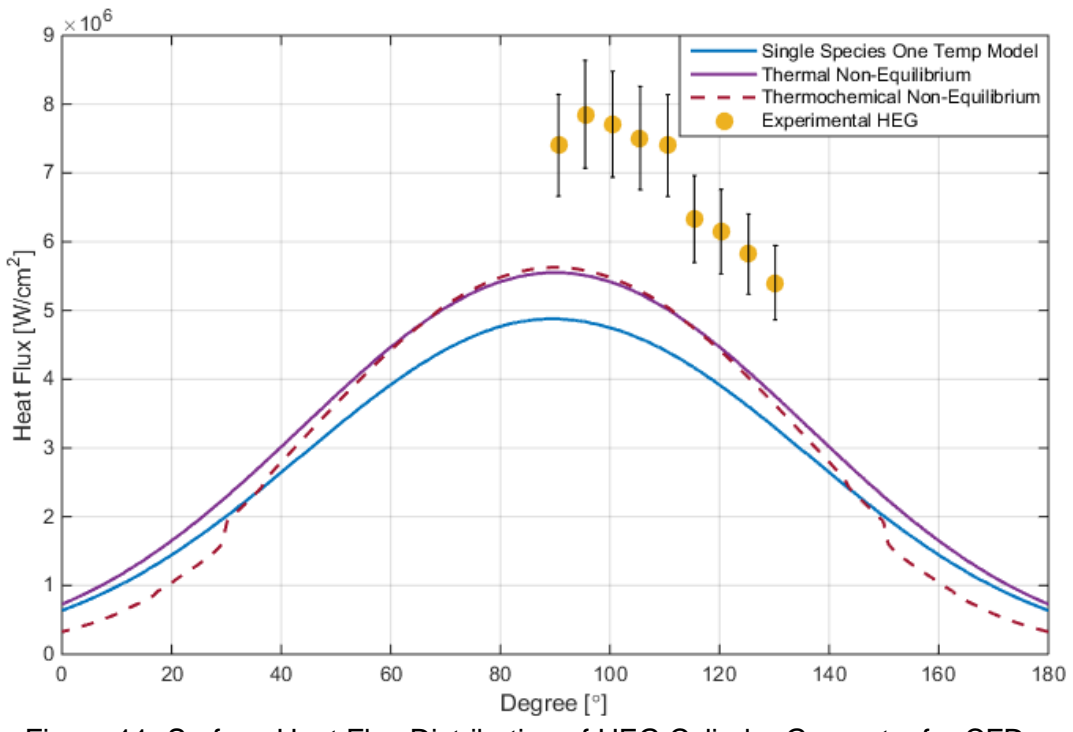


Figure 11- Surface Heat Flux Distribution of HEG Cylinder Geometry for CFD++

Figure 10 agrees with Fluent result because thermochemical nonequilibrium model predicts close to the experimental data. Moreover, other models are acceptably close as well. However, Figure 11 demonstrates that the best prediction is not close enough to the experimental data. The trend of simple model and thermal nonequilibrium model is as expected but thermochemical nonequilibrium model does not predict as close as Fluent's one.

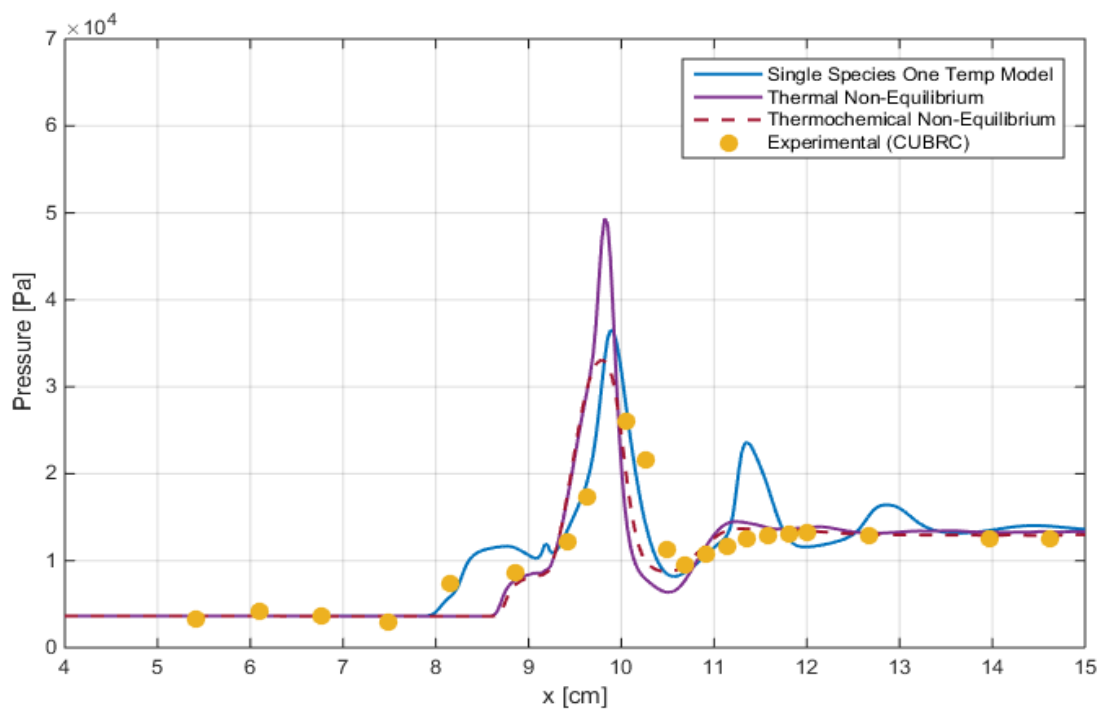


Figure 12- Surface Pressure Distribution of CUBRC Double Cone Geometry for CFD++

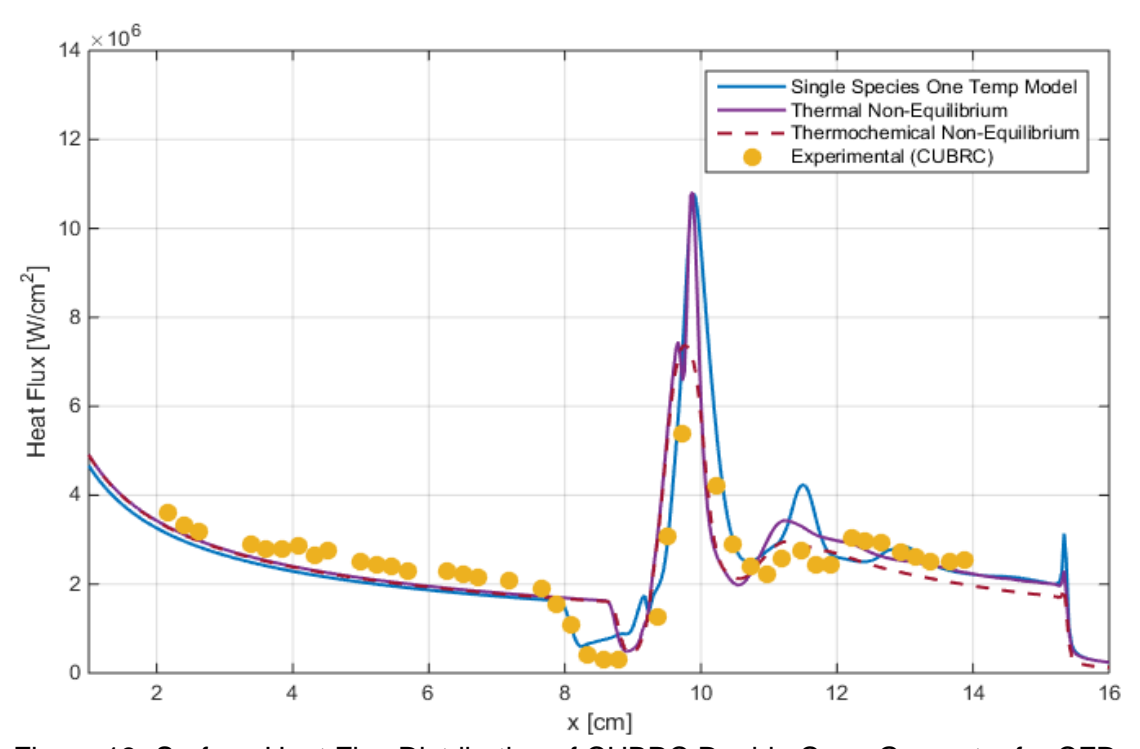


Figure 13- Surface Heat Flux Distribution of CUBRC Double Cone Geometry for CFD++

On the other hand, Figure 12 and Figure 13 indicates that thermochemical nonequilibrium model performs like Fluent for double cone geometry. There is a clear fluctuation for simple model, which should be investigated further. In general, CFD trend of CFD++ follows the experimental data except for spike regions where strong gradients and harsh aerothermal effects exist.

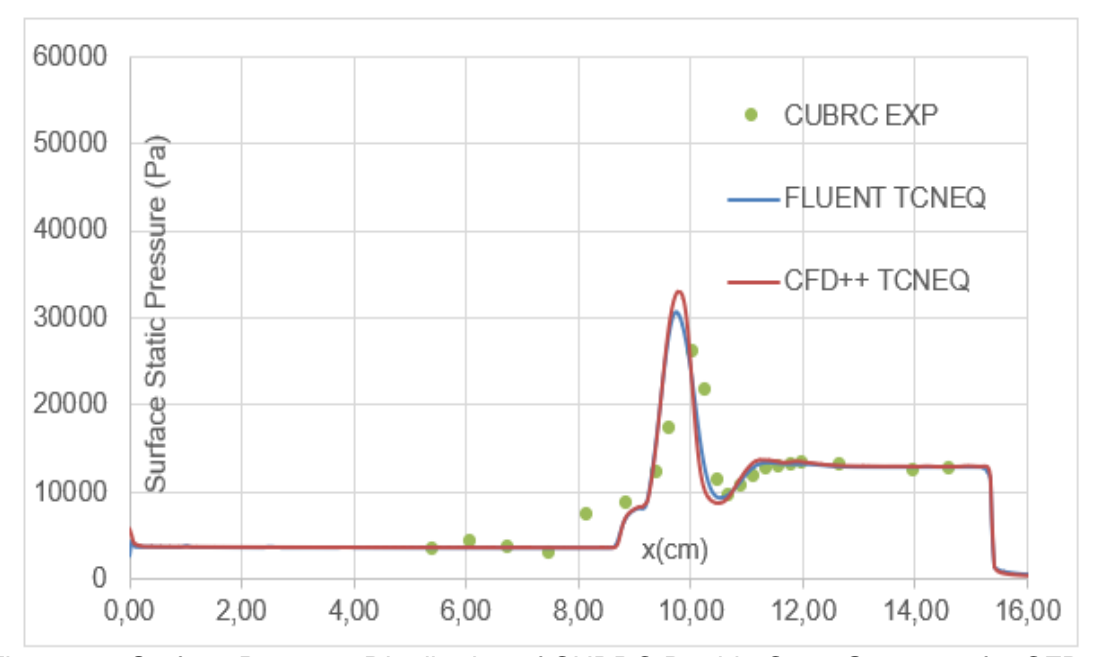


Figure 14- Surface Pressure Distribution of CUBRC Double Cone Geometry for CFD++

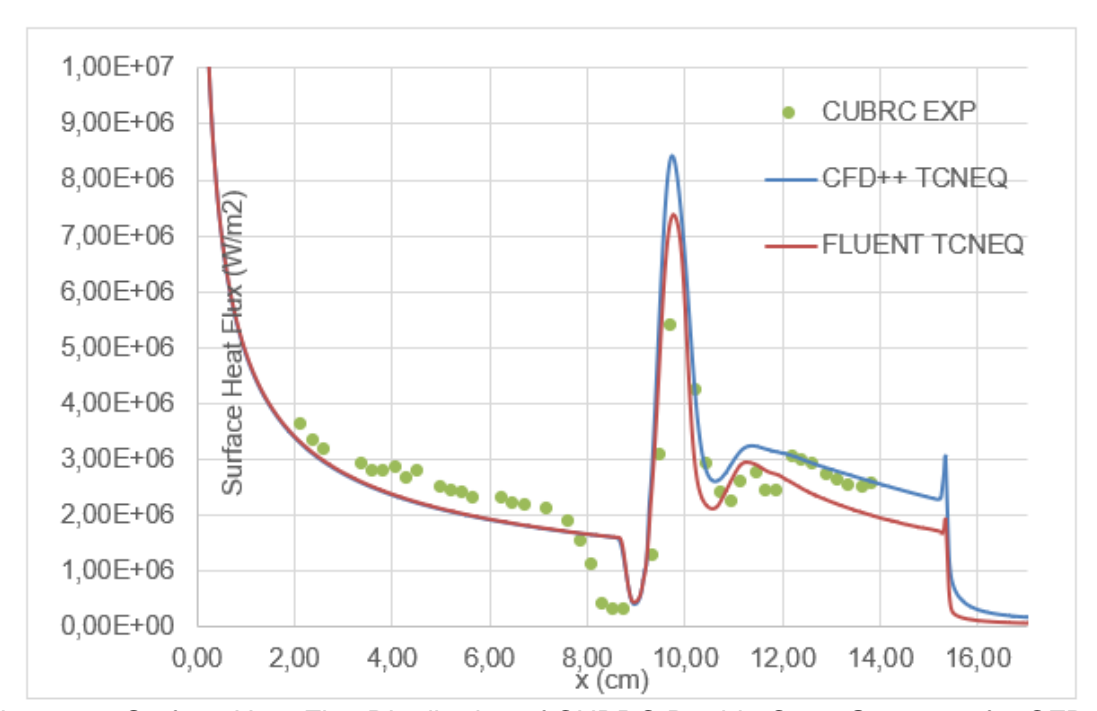


Figure 15- Surface Heat Flux Distribution of CUBRC Double Cone Geometry for CFD++

Figure 14 and Figure 15 summarize how two solvers behave when their thermochemical nonequilibrium models are used at double cone geometry. Both of surface pressure and heat flux trends agree with the experimental data and Fluent results seem slightly closer to experimental data. Secondly, both solvers predict the location of separation bubble slightly in front of the experimental data at 8-9 cm.

In the literature, there are additional research about these two geometries. Other than experimental data, similar CFD results can be examined to see where present CFD result stands. [2] and [7] and [8] includes many results about these geometries with similar freestream conditions. The amount of deviations and how trends are followed by present solvers strongly agree with literature results, especially for Fluent. Also, the literature indicates that CFD prediction can still be improved by introducing some additional effects such as catalytic wall condition.

4. Conclusion

In this research, the main purpose is the investigation and validation of two different solvers under high-enthalpy hypersonic flow conditions. The accurate predications are required to design, analysis and optimization phases of real 3D geometries. Results indicate that the general trend of experimental data can be followed by these commercial solvers. Since there are many challenging and hard to model physical phenomena at certain regions of geometries, there may exist some deviations. However, more complicated use of thermochemical nonequilibrium model decreases these deviations. Nevertheless, simpler models can give a general idea for trends and most of geometries except for certain locations. The choice of the model is a trade-off problem depending on computational resources and the level of required accuracy. Also, it should not be forgotten that CFD results are compared with some experimental data, which are taken from few locations. Physical data changes rapidly at locations with strong gradients and deviations, and one of the reasons of CFD deviations at these regions may be the spacing of the measurements. Further studies will aim improving the predication at every location of the surface and investigating root reasons of slight differences between two solvers.

5. Contact Author Email Address

mailto: sefa.dikmen@roketsan.com.tr

6. Copyright Statement

The authors confirm that they, and/or their company or organization, hold copyright on all of the original material included in this paper. The authors also confirm that they have obtained permission, from the copyright holder of any third-party material included in this paper, to publish it as part of their paper. The authors confirm that they give permission, or have obtained permission from the copyright holder of this paper, for the publication and distribution of this paper as part of the ICAS proceedings or as individual off-prints from the proceedings.

References

- [1] Zhang, W., Zhang, Z., Wang, X. *et.al.* A review of the mathematical modeling of equilibrium and nonequilibrium hypersonic flows. *Adv. Aerodyn.* 4, 38, 2022. https://doi.org/10.1186/s42774-022-00125-x
- [2] Knight, D., Longo, J., Drikakis, D., Gaitonde, D., Lani, A., Nompelis, I., Reimann, B., & Walpot, L. Assessment of CFD capability for prediction of hypersonic shock interactions. *Progress in Aerospace Sciences*, 48–49, 8–26, 2012. https://doi.org/10.1016/j.paerosci.2011.10.001
- [3] Rouhi Youssefi, M., & Knight, D. Assessment of CFD capability for hypersonic shock wave laminar boundary layer interactions. *Aerospace*, *4*(2), 25, 2017. https://doi.org/10.3390/aerospace4020025
- [4] Holden, M. S., Maclean M. Shock wave / laminar boundary layer interaction with real-gas effects presented at AIAA Aviation 2014. https://www.cubrc.org/index.php/page/publications/73-shock-wave-laminar-boundary-layer-interaction-with-real-gas-effects-presented-at-aiaa-aviation-2014
- [5] Park C. Review of chemical-kinetic problems of future NASA mission: Earth entries. Journal of Thermophysics and Heat Transfer 1993; 7:385–98, 1993.
- [6] Maier WT, Needels JT, Garbacz C, Morgado F, Alonso JJ, Fossati M. SU2-NEMO: An Open-Source Framework for High-Mach Nonequilibrium Multi-Species Flows. *Aerospace*.;8(7):193, 2021. https://doi.org/10.3390/aerospace8070193
- [7] Zuo, F.-Y., & Hu, S.-L. (2021). Thermochemical non-equilibrium effects on aerothermodynamic prediction of laminar double-cone flow. *Acta Astronautica*, 182, 179–188, 2021. https://doi.org/10.1016/j.actaastro.2021.01.058
- [8] Hao, J., Fan, J., Cao, S., & Wen, C.-Y. Three-dimensionality of hypersonic laminar flow over a double cone. *Journal of Fluid Mechanics*, *935*, 2021. https://doi.org/10.1017/jfm.2021.1137